Leading directions in the SMEFT: Renormalization effects

Admir Greljo,[*] Ajdin Palavrić,[†] and Aleks Smolkovič[‡]
Department of Physics, University of Basel, Klingelbergstrasse 82, CH-4056 Basel, Switzerland

(Received 18 December 2023; accepted 13 March 2024; published 16 April 2024)

The stability of the electroweak scale, challenged by the absence of deviations in flavor physics, prompts the consideration of SMEFT scenarios governed by approximate SM flavor symmetries. This study examines microscopic theories that match onto a set of $U(3)^5$-symmetric dimension-6 operators. Renormalization group (RG) mixing from the ultraviolet to the electroweak scale yields significant phenomenological constraints, particularly pronounced for UV-motivated directions. To demonstrate this, we explore a complete suite of tree-level models featuring new spin-0, spin-1/2, and spin-1 fields, categorized by their irreducible representations under the flavor group. We find that for the leading directions, corresponding to a single-mediator dominance, RG mixing effects occasionally serve as the primary indirect probe.

DOI: 10.1103/PhysRevD.109.075033

I. INTRODUCTION

Given a perceptible gap between the new physics (NP) scale and the electroweak (EW) scale, the Standard Model effective field theory (SMEFT) [1–6] emerges as a robust theoretical framework for describing deviations from the Standard Model (SM). The SMEFT Lagrangian is an infinite series of higher-dimensional local operators built from the SM fields obeying gauge and Poincaré symmetries. The respective Wilson coefficients (WCs) encapsulate the short-distance effects of a broad spectrum of models beyond the SM (BSM). In the absence of a clear direction toward a specific BSM scenario, such a framework provides a convincing path forward, informing phenomenological studies and data interpretation.

The minimal number of independent WCs (an operator basis) is rendered finite at each order in the inverse powers of the cutoff scale controlled by the canonical dimensions. Yet, the size of this space rapidly increases with the growing canonical dimension, but also with the number of families [7]. Specifically, for leading-order baryon-number conserving operators at dimension six, the parameter count rises from 59 for a single active generation to a striking 2499 for three generations [8]. This escalation underscores the complexity introduced by the flavor degrees of freedom.

On the other hand, the fermion kinetic terms enjoy a large $U(3)^5$ global symmetry owning to the three copies of five different gauge representations. The Yukawa interactions induce a rather peculiar explicit breaking, giving rise to exact and approximate flavor symmetries in the SM. The absence of violation of the implied selection rules in precision flavor experiments, such as $\Delta F = 2$ transitions, charged lepton flavor violation, and electric dipole moments, already imposes stringent constraints on NP which does not lie far above the EW scale [9]. Indeed, a viable TeV-scale physics, anticipated by the Higgs hierarchy problem and driving direct searches at the energy frontier, should not excessively violate the approximate flavor symmetries. This reasoning motivates the introduction of flavor power counting in the SMEFT, allowing for more focused analyses. Indeed, flavor symmetries prove to be very beneficial in charting the space of the SMEFT [10,11].

In this work, we consider a class of microscopic theories that integrate out to $U(3)^5$-symmetric dimension-6 basis made up of only 47 operators. These are the leading operators in the minimal flavor violation (MFV) [12] power counting and represent the most minimal complete operator basis of interest for global fits of top, Higgs, and electroweak data [13–16]. As such, it constitutes an important initial playground towards more complicated global analyses, such as those based on the $U(2)^5$ flavor symmetries [17–20].[1]

[*]admir.greljo@unibas.ch
[†]ajdin.palavric@unibas.ch
[‡]aleks.smolkovic@unibas.ch

[1]Smaller groups like $U(2)_{q+e}$ account for the peculiar fermion masses and mixings but offer limited protection against flavor constraints (see Fig. 1 in [21]).

Restricting ourselves to $U(3)^5$-symmetric operators at the ultraviolet (UV) matching scale, the main focus of this investigation is on the renormalization group (RG) effects between the UV and the EW scales. These effects are governed by the SMEFT anomalous dimension matrix computed in [8,22,23] (see also [24]) and implemented in numerical tools [25] such as `wilson` [26], DsixTools [27,28] and `RGESolver` [29]. While it has become a common practice to automatically include these effects, for example, in `smelli` [30], our work aims to pinpoint the most constrained linear combinations of operators at the UV matching scale resulting solely from RG mixing. To deepen the understanding of these effects, we provide simplified analytical expressions supported by the full numerical results. Our key interest lies in identifying RG-induced contributions to precision observables at low energies, which offer stronger or comparable bounds to those from tree-level processes. Upon examination, noteworthy cases involve four- and two-quark operators, where the RG bounds rival those from top quark production [31], echoing recent findings for top-specific operators [32].

To demonstrate the significance of RG effects, we examine a full set of tree-level mediator models matching onto the $U(3)^5$-symmetric operator basis at the UV scale. A complete spectrum of mediator fields with spin-0, spin-1/2, and spin-1, along with their SM and $U(3)^5$ flavor representations, has been comprehensively identified and matched to the universal basis in Ref. [33], building upon [34]. This matching process has defined a finite set of leading directions; UV-motivated linear combinations of the WCs, warranting thorough examination. This paper performs a complete RG analysis of all these leading directions, going beyond the tree-level phenomenology presented in [33]. Our central findings are showcased in Tables II–IV, comparing the RG bounds on a comprehensive set of four- and two-quark leading directions with the tree-level bounds.

This paper is structured as follows. In Sec. II we identify crucial RG equations, Sec. III gives an overview of the most sensitive low-energy observables, expressing them in terms of the WCs at the UV matching scale in the leading-log approximation. In Sec. IV, we derive a comprehensive set of bounds on the leading directions, which are then compared against exclusions from direct searches for selected benchmark models. The summary and the future outlook are presented in Sec. V.

II. RENORMALIZATION GROUP EFFECTS FROM FLAVOR-BLIND UV

The full $U(3)^5$-symmetric operator basis is defined in Appendix B of Ref. [33]. Focusing on the phenomenologically important RG effects, we consider a subset of operators at the UV matching scale involving quarks.[2] Our starting point is the Lagrangian,

$$\mathcal{L}_{\text{SMEFT}} \supset \sum_i C_i \mathcal{O}_i, \tag{1}$$

where the sum goes over all four-quark and two-quark-two-ϕ operators defined in Table I above the double line. Here, q and ℓ denote the left-handed quark and lepton doublets, while u and d denote the right-handed up- and down-quark fields. ϕ denotes the Higgs doublet. Flavor indices are $i, j = 1, 2, 3$, and the summation over repeated indices is

TABLE I. $U(3)^5$-symmetric dimension-6 SMEFT operators appearing at the UV matching scale in this work. The last four operators enter through the RG mixing. Our notation closely follows Ref. [33]. All operators considered are Hermitian, ensuring that their corresponding WCs are real.

Label	Operator
$\mathcal{O}_{qq}^{(1)D}$	$(\bar{q}_i\gamma^\mu q^i)(\bar{q}_j\gamma_\mu q^j)$
$\mathcal{O}_{qq}^{(3)D}$	$(\bar{q}_i\gamma^\mu\sigma^a q^i)(\bar{q}_j\gamma_\mu\sigma^a q^j)$
$\mathcal{O}_{qq}^{(1)E}$	$(\bar{q}_i\gamma^\mu q^j)(\bar{q}_j\gamma_\mu q^i)$
$\mathcal{O}_{qq}^{(3)E}$	$(\bar{q}_i\gamma^\mu\sigma^a q^j)(\bar{q}_j\gamma_\mu\sigma^a q^i)$
$\mathcal{O}_{dd}^{D}$	$(\bar{d}_i\gamma^\mu d^i)(\bar{d}_j\gamma_\mu d^j)$
$\mathcal{O}_{dd}^{E}$	$(\bar{d}_i\gamma^\mu d^j)(\bar{d}_j\gamma_\mu d^i)$
$\mathcal{O}_{uu}^{D}$	$(\bar{u}_i\gamma^\mu u^i)(\bar{u}_j\gamma_\mu u^j)$
$\mathcal{O}_{uu}^{E}$	$(\bar{u}_i\gamma^\mu u^j)(\bar{u}_j\gamma_\mu u^i)$
$\mathcal{O}_{ud}^{(1)}$	$(\bar{u}_i\gamma^\mu u^i)(\bar{d}_j\gamma_\mu d^j)$
$\mathcal{O}_{ud}^{(8)}$	$(\bar{u}_i\gamma^\mu T^A u^i)(\bar{d}_j\gamma_\mu T^A d^j)$
$\mathcal{O}_{qu}^{(1)}$	$(\bar{q}_i\gamma^\mu q^i)(\bar{u}_j\gamma_\mu u^j)$
$\mathcal{O}_{qu}^{(8)}$	$(\bar{q}_i\gamma^\mu T^A q^i)(\bar{u}_j\gamma_\mu T^A u^j)$
$\mathcal{O}_{qd}^{(1)}$	$(\bar{q}_i\gamma^\mu q^i)(\bar{d}_j\gamma_\mu d^j)$
$\mathcal{O}_{qd}^{(8)}$	$(\bar{q}_i\gamma^\mu T^A q^i)(\bar{d}_j\gamma_\mu T^A d^j)$
$\mathcal{O}_{\phi q}^{(1)}$	$(\phi^\dagger i\overleftrightarrow{D}_\mu\phi)(\bar{q}_i\gamma^\mu q^i)$
$\mathcal{O}_{\phi q}^{(3)}$	$(\phi^\dagger i\overleftrightarrow{D}^a_\mu\phi)(\bar{q}_i\gamma^\mu\sigma^a q^i)$
$\mathcal{O}_{\phi u}$	$(\phi^\dagger i\overleftrightarrow{D}_\mu\phi)(\bar{u}_i\gamma^\mu u^i)$
$\mathcal{O}_{\phi d}$	$(\phi^\dagger i\overleftrightarrow{D}_\mu\phi)(\bar{d}_i\gamma^\mu d^i)$
$\mathcal{O}_{\ell q}^{(3)}$	$(\bar{\ell}_i\gamma^\mu\sigma^a\ell^i)(\bar{q}_j\gamma_\mu\sigma^a q^j)$
$\mathcal{O}_{\ell\ell}^{E}$	$(\bar{\ell}_i\gamma^\mu\ell^j)(\bar{\ell}_j\gamma_\mu\ell^i)$
$\mathcal{O}_{\phi\ell}^{(3)}$	$(\phi^\dagger i\overleftrightarrow{D}^a_\mu\phi)(\bar{\ell}_i\gamma^\mu\sigma^a\ell^i)$
$\mathcal{O}_{\phi D}$	$(\phi^\dagger D_\mu\phi)[(D^\mu\phi)^\dagger\phi]$

[2]For all leading directions involving leptons, we have verified that tree-level effects consistently dominate (see Sec. IV). The same is true for purely bosonic operators with the exception of $\mathcal{O}_\phi$ already discussed in [33]. For interesting RG effects in semileptonic operators with generic flavor see [35].

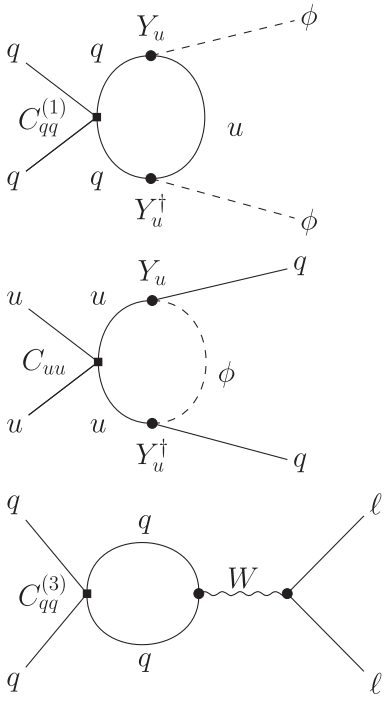

FIG. 1. Representative RG diagrams: See Sec. II for details.

assumed. In the rest of the paper, the labels assigned to the WCs, which we treat as dimensionful parameters, correspond directly to the labels of the operators from Table I.

Starting from Eq. (1) at the UV matching scale, the RG equations [8,22,23] determine the nonzero dimension-6 WCs at the EW scale, where the subsequent matching to the low-energy effective field theory (LEFT) [36] is performed at the tree level.[3] There are three categories of important RG effects depicted in Fig 1:

(i) Four-quark operator mixing into an EW boson vertex;
(ii) Four-quark operator mixing with two insertions of Yukawa interactions;
(iii) Four-quark operator mixing into a semileptonic operator.

While gauge interactions are flavor-diagonal (FD), the Yukawa-dependent part of the anomalous dimension matrix leads to FD and flavor-violating (FV) effects. For example, when matched to the LEFT, the resulting operators from category (i) produce both FD and FV Z couplings. The latter ones play a role in $\Delta F = 1$ processes such as $b \to s\ell\ell$ decays.[4]

[3]See Ref. [37] for one-loop matching effects in the flavor-symmetric SMEFT.

[4]We have verified that two insertions of FV Z couplings, effectively suppressed by $1/\Lambda^4$, as well as beyond the leading-log mixing of four-quark operators, yield subleading constraints from $\Delta F = 2$ processes compared to $\Delta F = 1$.

A. Vertex corrections

As depicted by the top diagram in Fig. 1, operators $\mathcal{O}_{qq}^{(1,3)}$ mix into $\mathcal{O}_{\phi q}^{(1,3)}$ by closing the loop with an up-type quark and emitting two Higgs fields. See Ref. [22] for the flavor-generic RG expressions. These contributions are proportional to $Y_u Y_u^\dagger$, leading to y_t^2-enhanced effects.[5]

All such effects, including the running of the operators from the $\psi^2 H^2 D$ class, can be described by the following set of RG equations:

$$\begin{aligned}
\dot{C}^{(1)}_{\substack{\phi q\\ pr}} &= C^{(1)}_{\phi q,\mathrm{FV}}[Y_u Y_u^\dagger]_{pr} + C^{(1)}_{\phi q,\mathrm{FD}}\delta_{pr},\\
\dot{C}^{(3)}_{\substack{\phi q\\ pr}} &= C^{(3)}_{\phi q,\mathrm{FV}}[Y_u Y_u^\dagger]_{pr} + C^{(3)}_{\phi q,\mathrm{FD}}\delta_{pr},\\
\dot{C}_{\substack{\phi u\\ pr}} &= C^{1}_{\phi u,\mathrm{FD}}[Y_u^\dagger Y_u]_{pr} + C^{2}_{\phi u,\mathrm{FD}}\delta_{pr},\\
\dot{C}_{\substack{\phi d\\ pr}} &= C_{\phi d,\mathrm{FD}}\delta_{pr},
\end{aligned} \tag{2}$$

where the abbreviation of the form $\dot{C} \equiv 16\pi^2\mu\frac{d}{d\mu}C$ is used, and we introduce the linear combinations of WCs in the flavor-symmetric basis[6]

$$\begin{aligned}
C^{(1)}_{\phi q,\mathrm{FV}} &\equiv 2C^{(1)D}_{qq} + 6C^{(3)D}_{qq} + 12C^{(1)E}_{qq} - C_{\phi u} + 4C^{(1)}_{\phi q} - 9C^{(3)}_{\phi q},\\
C^{(1)}_{\phi q,\mathrm{FD}} &\equiv \left(2C^{(1)E}_{qq} + 6C^{(3)E}_{qq} + 12C^{(1)D}_{qq} - 6C^{(1)}_{qu} + 6C^{(1)}_{\phi q}\right)y_t^2,\\
C^{(3)}_{\phi q,\mathrm{FV}} &\equiv -2C^{(1)D}_{qq} + 2C^{(3)D}_{qq} - 12C^{(3)E}_{qq} - 3C^{(1)}_{\phi q} + 2C^{(3)}_{\phi q},\\
C^{(3)}_{\phi q,\mathrm{FD}} &\equiv -2\left(C^{(1)E}_{qq} - C^{(3)E}_{qq} + 6C^{(3)D}_{qq} - 3C^{(3)}_{\phi q}\right)y_t^2\\
&\quad + \frac{g_2^2}{3}\left(2C^{(1)D}_{qq} + 6C^{(1)E}_{qq} + 34C^{(3)D}_{qq} + 6C^{(3)E}_{qq} + C^{(3)}_{\phi q}\right),\\
C^{1}_{\phi u,\mathrm{FD}} &\equiv -12C^{E}_{uu} - 4C^{D}_{uu} - 2C^{(1)}_{\phi q} + 8C_{\phi u},\\
C^{2}_{\phi u,\mathrm{FD}} &\equiv 2\left(3C^{(1)}_{qu} - 6C^{D}_{uu} - 2C^{E}_{uu} + 3C_{\phi u}\right)y_t^2,\\
C_{\phi d,\mathrm{FD}} &\equiv 6\left(C^{(1)}_{qd} - C^{(1)}_{ud} + C_{\phi d}\right)y_t^2.
\end{aligned} \tag{3}$$

When the operators $\mathcal{O}_{\phi q}^{(1,3)}$, $\mathcal{O}_{\phi u}$, and $\mathcal{O}_{\phi d}$, generated via Eq. (2), are matched to the LEFT, they induce modified Z and W couplings to quarks [36], contributing to important FD, as well as FV observables (see Sec. III).

B. Four-quark operators

The four-quark operators given in Table I mix among themselves under RG equations, leading to interesting

[5]Throughout this work, we will not discuss small contributions $\propto Y_d Y_d^\dagger$, although they are included in our numerical studies.

[6]We omit contributions proportional to g_1 and smaller parameters, although they are fully included in the numerical analyses of Sec. IV.

$\Delta F = 1$ FV effects as illustrated by the middle diagram in Fig. 1. The system of equations, simplified to include only Y_u-dependent terms, is as follows:

$$\dot{C}^{(1)}_{\substack{qu\\prst}} = C^{(1)}_{qu,\mathrm{FV}}[Y_u Y_u^\dagger]_{pr}\delta_{st}, \qquad \dot{C}^{(1)}_{\substack{qd\\prst}} = C^{(1)}_{qd,\mathrm{FV}}[Y_u Y_u^\dagger]_{pr}\delta_{st},$$
$$\dot{C}^{(8)}_{\substack{qu\\prst}} = C^{(8)}_{qu,\mathrm{FV}}[Y_u Y_u^\dagger]_{pr}\delta_{st}, \qquad \dot{C}^{(8)}_{\substack{qd\\prst}} = C^{(8)}_{qd,\mathrm{FV}}[Y_u Y_u^\dagger]_{pr}\delta_{st}, \tag{4}$$

where we introduce the linear combinations

$$C^{(1)}_{qu,\mathrm{FV}} \equiv C^{(1)}_{qu} - \frac{2}{3}C^{E}_{uu} - 2C^{D}_{uu}, \qquad C^{(1)}_{qd,\mathrm{FV}} \equiv C^{(1)}_{qd} - C^{(1)}_{ud},$$
$$C^{(8)}_{qu,\mathrm{FV}} \equiv C^{(8)}_{qu} - 4C^{E}_{uu}, \qquad C^{(8)}_{qd,\mathrm{FV}} \equiv C^{(8)}_{qd} - C^{(8)}_{ud}. \tag{5}$$

As in previous cases, these are formulated in terms of the WCs of operators from the flavor-symmetric basis. The RG equations presented here are not exhaustive but capture only the phenomenologically relevant terms.

C. Semileptonic operators

For the upcoming analysis of the low-energy observables, as it unfolds, keeping only the RG terms proportional to g_2^2, while neglecting the ones proportional to g_1^2, there is only one relevant RG-generated semileptonic operator, which appears as a result of the $\mathcal{O}^{(3)}_{qq}$ mixing into $\mathcal{O}^{(3)}_{\ell q}$ [8]. The RG equation for $\mathcal{O}^{(3)}_{\ell q}$ operator takes the form

$$\dot{C}^{(3)}_{\substack{\ell q\\prst}} = g_2^2 C^{(3)}_{\ell q,\mathrm{FD}}\delta_{pr}\delta_{st}, \tag{6}$$

where we introduce

$$C^{(3)}_{\ell q,\mathrm{FD}} \equiv \frac{2}{3}\left(C^{(1)D}_{qq} + 3C^{(1)E}_{qq} + 17C^{(3)D}_{qq} + 3C^{(3)E}_{qq}\right). \tag{7}$$

To reemphasize, our numerical analysis in Sec. IV does not employ such approximations. Nonetheless, the above equations effectively approximate the most sensitive RG effects.

III. RG-INDUCED LOW-ENERGY PROBES

Having detailed the relevant RG equations, this section focuses on their impact on key low-energy probes. We address this by solving these equations using a leading-log approximation, which allows us to express low-energy (pseudo)-observables in terms of the WCs at the UV matching scale.

A. $b \to s\ell\ell$

Flavor-violating Z couplings to quarks, represented by the $\mathcal{O}^{(1,3)}_{\phi q}$ matching to LEFT, are effectively constrained from rare meson decays to charged leptons or neutrinos.[7] Presently, available data from charged leptons is more constraining, while final states with neutrinos can provide a complementary test in the future. Furthermore, correlated effects are predicted in all down-quark FV neutral currents, including $b \to s$, $b \to d$, and $s \to d$ transitions. In fact, the measurements of $b \to s\ell\ell$ decays provide the most sensitive probe of semileptonic interactions with MFV structure, see Ref. [38].

Rare b decays are described by the weak Hamiltonian,

$$\mathcal{H}_{\mathrm{eff.}} \supset -\frac{4G_F}{\sqrt{2}}\frac{\alpha}{4\pi}V^*_{ts}V_{tb}(C_9\mathcal{O}_9 + C_{10}\mathcal{O}_{10}) + \mathrm{H.c.}, \tag{8}$$

where G_F is the Fermi constant and α is the fine-structure constant, while the local operators are defined as

$$\mathcal{O}_9 = (\bar{\ell}\gamma_\mu\ell)(\bar{s}_L\gamma^\mu b_L), \qquad \mathcal{O}_{10} = (\bar{\ell}\gamma_\mu\gamma_5\ell)(\bar{s}_L\gamma^\mu b_L), \tag{9}$$

and $C_{9,10}$ denote the short-distance contributions. NP contributions through modified Z couplings to quarks predict lepton flavor universality. In addition, C_9^{NP} is suppressed due to the small Z couplings to the leptonic vector current. Conversely, C_{10}^{NP} receives significant NP contributions.

After solving the RG equations (2) in the leading-log approximation and matching SMEFT onto LEFT at the tree level, we find,

$$C_{10}^{\mathrm{NP}} = -\frac{v^2}{4e^2}y_t^2(C^{(1)}_{\phi q,\mathrm{FV}} + C^{(3)}_{\phi q,\mathrm{FV}})\ln\left(\frac{\mu_i}{\mu_f}\right), \tag{10}$$

where $v \approx 246$ GeV is the Higgs vacuum expectation value, e is the elementary charge, $\mu_f = m_Z$ is the EW matching scale, and $\mu_i = \mathcal{O}(\mathrm{TeV})$ is the UV matching scale.[8] In the following, we will use C_{10}^{NP} as a pseudo-observable, contrasting it with the best-fit interval from global fits to $b \to s\ell\ell$ data, $C_{10}^{\mathrm{NP}} = 0.23 \pm 0.15$ [38], see also [39–42] (see e.g., Appendix B of Ref. [39] for a list of observables entering such analyses).

B. ε'/ε

The ε'/ε ratio measures the size of direct ($\Delta F = 1$) CP violation in $K_L \to \pi\pi$ relative to indirect ($\Delta F = 2$) CPV. The current experimental world average is $(\epsilon'/\epsilon)_{\mathrm{exp}} = (16.6 \pm 2.3) \times 10^{-4}$ [43]. As for the SM prediction, we take the current best estimate as $(\epsilon'/\epsilon)_{\mathrm{SM}} = (13.9 \pm 5.2) \times 10^{-4}$ [44–48].

[7] Down-quark FV is absent when $C^{(1)}_{\phi q} = -C^{(3)}_{\phi q}$ at the EW scale.

[8] Note, that finite one-loop matching contributions are subleading when compared to large log-enhanced RG effects [13,37].

In our framework, contributions to this observable are generated by the RG mixing of the four-quark operators (Sec. II B), along with the four-quark operators mixing into the gauge boson vertex corrections (Sec. II A). Solving the RG equations (2) and (4) in the leading-log approximation, then matching the SMEFT onto the JMS LEFT basis [36], and using the master formula provided in [47,49] we obtain,

$$\begin{aligned}(\varepsilon'/\varepsilon)_{\rm BSM} = -N_{\Delta S=1}\frac{y_t^2}{16\pi^2}\ln\left(\frac{\mu_i}{\mu_f}\right)\mathrm{Im}[V_{ts}^* V_{td}] \\ \times\Bigg\{\left[C^{(1)}_{qu,\rm FV} - \frac{4}{3}s_\theta^2\left(C^{(1)}_{\phi q,\rm FV} + C^{(3)}_{\phi q,\rm FV}\right)\right]P^{(1)}_{du} \\ + \left[C^{(1)}_{qd,\rm FV} + \frac{2}{3}s_\theta^2\left(C^{(1)}_{\phi q,\rm FV} + C^{(3)}_{\phi q,\rm FV}\right)\right]P^{(1)}_{dd} \\ + C^{(8)}_{qu,\rm FV}P^{(8)}_{du} + C^{(8)}_{qd,\rm FV}P^{(8)}_{dd}\Bigg\},\end{aligned} \tag{11}$$

where $\mathcal{N}_{\Delta S=1} = (1\ \mathrm{TeV})^2$. We only keep the contributions from the largest hadronic matrix elements, $P^{(1,8)}_{dd} \equiv P[C^{V(1,8),LR}_{dd\,2111}]$, $P^{(1,8)}_{du} \equiv P[C^{V(1,8),LR}_{du\,2111}]$ [47], which capture all of the relevant effects in this study. Note that, in accordance with the aforementioned references, $\mu_f = 160$ GeV is used. As a final comment, although we start with strictly real WCs at the UV scale (see e.g., Ref. [50] for a discussion regarding imaginary WCs), through the process of RG mixing and matching, we end up with $\mathrm{Im}[V_{ts}^* V_{td}]$, which then enters the CP-violating observable ε'/ε.[9]

C. W mass

We choose (G_F, m_Z, α) as an input parameter set and can therefore predict the value of m_W both in the SM, including up to two-loop corrections [51], and in $U(3)^5$-symmetric SMEFT [52–54]. We express the combined prediction as $m_W^2 = m_{W,\rm SM}^2 + \delta m_W^2$ with

$$\frac{\delta m_W^2}{m_W^2} = -\frac{v^2 s_{2\theta}}{4c_{2\theta}}\left[\frac{c_\theta}{s_\theta}C_{\phi D} + \frac{s_\theta}{c_\theta}\left(4C^{(3)}_{\phi l} - 2C^E_{ll}\right)\right], \tag{12}$$

where θ is the Weinberg angle, $s_x \equiv \sin x$, and $c_x \equiv \cos x$.[10]

The operator class $\psi^2 H^2 D^2$ from the $U(3)^5$-symmetric basis (where ψ denotes quark fields) contributes to m_W already at the leading log, by mixing into $\mathcal{O}_{\phi D}$ and $\mathcal{O}^{(3)}_{\phi\ell}$. The corresponding RG equations are given as

$$\dot{C}_{\phi D} = 24y_t^2\left(C^{(1)}_{\phi q} - C_{\phi u}\right), \qquad \dot{C}^{(3)}_{\substack{\phi\ell\\ rs}} = 6g_2^2 C^{(3)}_{\phi q}\delta_{rs}. \tag{13}$$

Solving these equations, we find

$$\frac{\delta m_W^2}{m_W^2} = \frac{3v^2}{8\pi^2}\frac{s_{2\theta}}{c_{2\theta}}\ln\left(\frac{\mu_i}{\mu_f}\right)\left[y_t^2\frac{c_\theta}{s_\theta}\left(C^{(1)}_{\phi q} - C_{\phi u}\right) + g_2^2\frac{s_\theta}{c_\theta}C^{(3)}_{\phi q}\right]. \tag{14}$$

Interestingly, the four-quark operators considered in this work only contribute to δm_W^2 beyond the leading-log approximation. Specifically, all four-quark operators in Table I except color octets contribute at this order.[11] For example, $\mathcal{O}(Y_u^4)$ contribution proceeds through $C^{D,E}_{uu} \to C_{\phi u} \to C_{\phi D}$ and similarly at $\mathcal{O}(g_2^4)$, we have $C^{(3)D,E}_{qq} \to C^{(3)}_{\ell q} \to C^{D,E}_{\ell\ell}$. Here, we rely on a fully numerical solution of the RG equations using `wilson` [26].

We use `flavio` [55] to obtain the SM prediction, $m_W^{\rm SM} = (80.355 \pm 0.005)$ GeV. As for the measured value, we consider the latest PDG combination of $m_W^{\rm exp.} = (80.377 \pm 0.012)$ GeV [43], which does not include the anomalous CDF II result [56].

D. Z-pole observables

As discussed in Sec. II A, the operators considered in this work can lead to modifications of the FD Z-boson couplings with quarks. Such effects can be constrained from electroweak precision tests (EWPT) with on shell Z bosons [57,58]. These constitute various partial decay width ratios, forward-backward asymmetries, and left-right asymmetries [57,59]. We utilize an extensive list of observables with correlated experimental errors, employing `smelli` [30] to build a custom EWPT likelihood focused solely on Z-pole observables (see, e.g., Table 1 in Ref. [57] for a list of observables). We exclude m_W (analyzed separately in Sec. III C) and W-pole observables sensitive to modified W couplings to SM fermions, as they are not phenomenologically competitive. The constructed likelihood relies crucially on `flavio` [55] due to its database of experimental measurements [43,59–61] and the implemented theoretical predictions of the considered observables at the scale $\mu = m_Z$, including SM and BSM contributions [3,62]. In the subsequent numerical analysis, we use `wilson` [26] to run and match the WCs, also capturing beyond leading-log effects, and collectively denote the resulting limits with δg_Z.

[9]This effect is independent of the flavor basis used. In the up basis, two CKM matrix element insertions arise when rotating d quarks to mass eigenstates, while in the down basis, they emerge from rotating the Y_u matrix in the RG equations.

[10]It should be noted that Eq. (12) generally includes an additional term proportional to $C_{\phi WB}$ [52–54]. However, operators from Table I do not mix into this operator at the one-loop level.

[11]Color octets are absent because loops with color octet operator insertions in the relevant mixing cascades are always proportional to $\mathrm{Tr}(T^A)$, which is identically zero.

E. β-decays

Following the discussion in Sec. II, the only RG contributions to charged-current processes in our framework go through either modified W couplings with left-handed quarks due to $\mathcal{O}^{(3)}_{\phi q}$, see Eq. (2), or through the $\mathcal{O}^{(3)}_{\ell q}$ contact interaction, see Eq. (6). Both of these match onto the same low-energy $V-A$ operator. The low-energy Hamiltonian is

$$\mathcal{H}_{\rm eff} \supset \frac{4G_F}{\sqrt{2}} \sum_{x=d,s,b} \tilde{V}_{ux}(\bar{u}_L\gamma_\mu x_L)(\bar{e}_L\gamma_\mu \nu_{eL}) + \text{H.c.}. \quad (15)$$

The NP contributions to the left-handed currents have been absorbed into $\tilde{V}_{ux}$ as $\tilde{V}_{ux} = V_{ux}(1+\epsilon^x_L)$, where V_{ux} are elements of the unitary rotation matrix [63,64]. The effects of nonzero ϵ^x_L can be probed through the violation of the (first row)Cabibbo-Kobayashi-Maskawa (CKM) unitarity,

$$\Delta_{\rm CKM} \equiv |\tilde{V}_{ud}|^2 + |\tilde{V}_{us}|^2 + |\tilde{V}_{ub}|^2 - 1. \quad (16)$$

Solving the respective RG equations in the leading-log approximation and matching onto Eq. (15) we obtain,

$$\epsilon^x_L = \frac{v^2}{16\pi^2}(g_2^2 C^{(3)}_{\ell q,\rm FD} - C^{(3)}_{\phi q,\rm FD}) \ln\left(\frac{\mu_i}{\mu_f}\right), \quad (17)$$

for all $x = d, s, b$. The CKM unitarity test then reduces to $\Delta_{\rm CKM} \approx 2\epsilon^x_L$ at linear order in WCs, with no summation over x.

The most accurate value of $|\tilde{V}_{ud}|$ is from superallowed β decays, taken as the latest PDG average of $(0.97373 \pm 0.00031$ [43,65]. For $|\tilde{V}_{us}|$, we use the conservative PDG average of semileptonic kaon decays and the kaon-to-pion decay ratio, at 0.2243 ± 0.0008 [43]. Including the minor $|\tilde{V}_{ub}| = (3.82 \pm 0.20) \times 10^{-3}$ contribution, the experimental constraint is $\Delta^{\rm exp.}_{\rm CKM} = (-1.52 \pm 0.70) \times 10^{-3}$, reflecting the known Cabibbo angle anomaly [66–70].

F. Atomic parity violation

Atomic parity violation (APV) is sensitive to parity-violating couplings of electrons to quarks. Experiments report the weak charge, defined as

$$Q_{\rm W}(Z,N) = -2[(2Z+N)g^{eu}_{\rm AV} + (Z+2N)g^{ed}_{\rm AV}], \quad (18)$$

where Z (N) is the number of protons (neutrons). The general expressions for $g^{eu}_{\rm AV}$ and $g^{ed}_{\rm AV}$ are given in [63]. Upon solving the RG equations (2) and (6) in the leading-log approximation we get,

$$\begin{aligned} g^{eu}_{\rm AV} &\equiv -\frac{1}{2} + \frac{4}{3}s^2_\theta + \frac{v^2}{32\pi^2}\ln\left(\frac{\mu_i}{\mu_f}\right) \\ &\quad \times \left\{-g_2^2 C^{(3)}_{lq,\rm FD} - C^2_{\phi u,\rm FD} + C^{(3)}_{\phi q,\rm FD} - C^{(1)}_{\phi q,\rm FD}\right\}, \\ g^{ed}_{\rm AV} &\equiv \frac{1}{2} - \frac{2}{3}s^2_\theta + \frac{v^2}{32\pi^2}\ln\left(\frac{\mu_i}{\mu_f}\right) \\ &\quad \times \left\{g_2^2 C^{(3)}_{lq,\rm FD} - C_{\phi d,\rm FD} - C^{(3)}_{\phi q,\rm FD} - C^{(1)}_{\phi q,\rm FD}\right\}. \end{aligned} \quad (19)$$

The most precise measurements are done with the cesium (^{133}Cs) atom, for which

$$Q^{\rm Cs}_{\rm W} \approx -376 g^{eu}_{\rm AV} - 422 g^{ed}_{\rm AV}, \quad (20)$$

up to small radiative corrections [71–73]. The prediction for the cesium weak charge obtained in the SM is $Q^{\rm Cs,SM}_{\rm W} = -73.23(1)$ [72–74] which includes radiative corrections, while the current experimental value as reported by PDG is $Q^{\rm Cs,exp.}_{\rm W} = -72.82(42)$ [72,75,76].

IV. LEADING DIRECTIONS

The natural next step in a systematic bottom-up approach is to construct UV completions of the $U(3)^5$-symmetric dimension-6 basis. An exhaustive leading-order classification yields a finite set of possibilities within the scope of perturbative short-distance NP. The UV/IR dictionary of Ref. [34] is a collection of all possible SM gauge representations of new scalar, fermion, and vector fields that match onto dimensions-6 operators in the SMEFT at the tree level. Expanding on this, Ref. [33] further imposed $U(3)^5$ flavor symmetry to the UV Lagrangian, categorizing new mediator fields into irreducible representations (irreps) and defining the flavor coupling tensors. The exact symmetry limit is highly predictable—each nontrivial flavor multiplet leads to mass degenerate states, which once integrated out, match to a single Hermitian operator in the $U(3)^5$-symmetric basis with a well-defined sign for the obtained WC.[12] Each case predicts a direction in the WC parameter space, denoted as a leading direction. A general tree-level matching result is a linear combination of these directions.

Needless to say, a finite number of scenarios featuring a single mediator dominance is of particular phenomenological importance. To this purpose, Ref. [33] conducted a thorough tree-level analysis for each leading direction, reporting a compendium of bounds based on the available data. This study extends the previous analysis by incorporating the RG effects. Upon a detailed case-by-case examination, we find that a substantial number of scenarios

[12]Even for trivial flavor irreps, a notable simplification occurs, with only a few instances involving more than one parameter, see Tables 4 and 5 in [33].

TABLE II. Scalar mediators: In the first column, we collect the labels for each mediator along with their irreps. under the SM gauge group. In the second column, we list the flavor irreps, while in the third and fourth columns, we provide the normalization and the linear combination of the generated operators from the $U(3)^5$-symmetric basis (see Table I). In the remaining columns we collect the 95% CL limits on the mass-to-coupling ratios (in TeV) from constraints discussed in Sec. IV A.

Scalars											
Field	Irrep	Normalization	Direction	Top	$b \to s\ell\ell$	ε'/ε	δg_Z	β	Q_W^{Cs}	m_W	Combined
$\varphi \sim (\mathbf{1},\mathbf{2})_{\frac{1}{2}}$	$(\bar{\mathbf{3}}_d,\mathbf{3}_q)$	$-\lvert y_\varphi^d\rvert^2/(6M_\varphi^2)$	$\mathcal{O}_{qd}^{(1)} + 6\mathcal{O}_{qd}^{(8)}$	1.0	⋯	0.8	0.8	⋯	0.7	0.3	1.2
	$(\bar{\mathbf{3}}_q,\mathbf{3}_u)$	$-\lvert y_\varphi^u\rvert^2/(6M_\varphi^2)$	$\mathcal{O}_{qu}^{(1)} + 6\mathcal{O}_{qu}^{(8)}$	1.7	0.4	1.0	0.8	⋯	0.5	0.9	1.8
$\omega_1 \sim (\mathbf{3},\mathbf{1})_{-\frac{1}{3}}$	$\bar{\mathbf{6}}_q$	$\lvert y_{\omega_1}^{qq}\rvert^2/(4M_{\omega_1}^2)$	$\mathcal{O}_{qq}^{(1)D} - \mathcal{O}_{qq}^{(3)D} + \mathcal{O}_{qq}^{(1)E} - \mathcal{O}_{qq}^{(3)E}$	1.8	3.6	0.7	2.9	[1.3, 6.4]	0.8	1.6	4.0
	$(\bar{\mathbf{3}}_d,\bar{\mathbf{3}}_u)$	$\lvert y_{\omega_1}^{du}\rvert^2/(3M_{\omega_1}^2)$	$\mathcal{O}_{ud}^{(1)} - 3\mathcal{O}_{ud}^{(8)}$	1.1	⋯	0.8	0.9	⋯	0.9	0.4	1.5
$\omega_2 \sim (\mathbf{3},\mathbf{1})_{\frac{2}{3}}$	$\mathbf{3}_d$	$\lvert y_{\omega_2}\rvert^2/M_{\omega_2}^2$	$\mathcal{O}_{dd}^{D} - \mathcal{O}_{dd}^{E}$	0.4	⋯	⋯	0.4	⋯	⋯	⋯	0.5
$\omega_4 \sim (\mathbf{3},\mathbf{1})_{-\frac{4}{3}}$	$\mathbf{3}_u$	$\lvert y_{\omega_4}^{uu}\rvert^2/M_{\omega_4}^2$	$\mathcal{O}_{uu}^{D} - \mathcal{O}_{uu}^{E}$	1.8	⋯	1.3	1.1	⋯	1.7	0.3	1.9
$\zeta \sim (\mathbf{3},\mathbf{3})_{-\frac{1}{3}}$	$\mathbf{3}_q$	$\lvert y_\zeta^{qq}\rvert^2/(2M_\zeta^2)$	$3\mathcal{O}_{qq}^{(1)D} + \mathcal{O}_{qq}^{(3)D} - 3\mathcal{O}_{qq}^{(1)E} - \mathcal{O}_{qq}^{(3)E}$	3.1	2.5	0.8	1.2	4.1	2.0	0.5	3.7
$\Omega_1 \sim (\mathbf{6},\mathbf{1})_{\frac{1}{3}}$	$(\mathbf{3}_u,\mathbf{3}_d)$	$\lvert y_{\Omega_1}^{ud}\rvert^2/(6M_{\Omega_1}^2)$	$2\mathcal{O}_{ud}^{(1)} + 3\mathcal{O}_{ud}^{(8)}$	1.0	⋯	0.5	0.8	⋯	0.9	0.3	1.4
	$\bar{\mathbf{3}}_q$	$\lvert y_{\Omega_1}^{qq}\rvert^2/(4M_{\Omega_1}^2)$	$\mathcal{O}_{qq}^{(1)D} - \mathcal{O}_{qq}^{(3)D} - \mathcal{O}_{qq}^{(1)E} + \mathcal{O}_{qq}^{(3)E}$	2.1	2.5	0.9	2.4	[1.7, 8.3]	1.1	0.6	2.6
$\Omega_2 \sim (\mathbf{6},\mathbf{1})_{-\frac{2}{3}}$	$\mathbf{6}_d$	$\lvert y_{\Omega_2}\rvert^2/(4M_{\Omega_2}^2)$	$\mathcal{O}_{dd}^{D} + \mathcal{O}_{dd}^{E}$	0.2	⋯	⋯	0.3	⋯	⋯	⋯	0.3
$\Omega_4 \sim (\mathbf{6},\mathbf{1})_{\frac{4}{3}}$	$\mathbf{6}_u$	$\lvert y_{\Omega_4}\rvert^2/(4M_{\Omega_4}^2)$	$\mathcal{O}_{uu}^{D} + \mathcal{O}_{uu}^{E}$	1.3	0.3	1.0	0.8	⋯	1.1	1.7	2.1
$\Upsilon \sim (\mathbf{6},\mathbf{3})_{\frac{1}{3}}$	$\mathbf{6}_q$	$\lvert y_\Upsilon\rvert^2/(8M_\Upsilon^2)$	$3\mathcal{O}_{qq}^{(1)D} + \mathcal{O}_{qq}^{(3)D} + 3\mathcal{O}_{qq}^{(1)E} + \mathcal{O}_{qq}^{(3)E}$	1.7	3.0	0.7	2.8	2.7	1.3	2.2	4.8
$\Phi \sim (\mathbf{8},\mathbf{2})_{\frac{1}{2}}$	$(\bar{\mathbf{3}}_q,\mathbf{3}_u)$	$-\lvert y_\Phi^{qu}\rvert^2/(18M_\Phi^2)$	$4\mathcal{O}_{qu}^{(1)} - 3\mathcal{O}_{qu}^{(8)}$	1.2	0.2	0.1	0.9	⋯	0.5	1.0	1.5
	$(\bar{\mathbf{3}}_d,\mathbf{3}_q)$	$-\lvert y_\Phi^{dq}\rvert^2/(18M_\Phi^2)$	$4\mathcal{O}_{qd}^{(1)} - 3\mathcal{O}_{qd}^{(8)}$	0.8	⋯	0.1	0.8	⋯	0.7	0.3	1.2

have RG-induced bounds competitive with tree-level bounds. These cases, along with their tree-level matching formulas, are presented in Table II for scalars, Table III for vectors, and Table IV for fermions.

These tables explain our initial choice of operators in Table I. The tree-level bounds on the UV mediators which match onto the four-quark operators (scalars and vectors) are from the top-quark production [31], while those generating two-quark-two-ϕ operators (fermions) were constrained from a combined low-energy fit of (semi) leptonic operators [63]. In Sec. IV A, we compare the tree-level with the RG-improved constraints for all mediators where the latter are numerically important.[13] In Sec. IV B, we finally compare these indirect constraints with direct searches for two benchmark cases, revealing an interesting interplay.

A. Improved EFT limits

In this section, we derive a set of RG-improved bounds on all leading directions in the operator space of Table I. In Sec. III, the observables are calculated using the leading-log approximation to elucidate RG-induced effects. However, the results presented here rely on solving the RG equations numerically. This approach, as compared to leading-log expressions, offers several improvements. It includes effects beyond the leading log, such as δm_W^2 from four-quark operators discussed in Sec. III C, ensures resummation of large logs, and accounts for terms proportional to g_1 and other smaller parameters, which were omitted in the leading-log expressions but are included in numerical calculations.

We use the open-source PYTHON package `wilson` [26] to numerically solve the RG equations.[14] The UV matching scale is set at $\mu_i = 3$ TeV, and we run down to low-energy scales, relevant for the observables discussed in Sec. III.[15] We separately construct χ^2 functions for each observable and a combined χ^2, considering both theoretical and experimental uncertainties. These functions are then used to derive 95% CL constraints on the effective mass of each mediator, represented as a mass-to-coupling ratio. If a single number is presented, it is to be understood as a lower

[13]Unlike tree-level bounds, RG-induced bounds depend on the UV renormalization scale μ_i, although this dependence is only logarithmic. In contrast, their dependence on the mass M_X and coupling y_X is quadratic, scaling as $\propto y_X^2/M_X^2$.

[14]We checked that our leading-log formula nicely agree with `wilson` where appropriate.

[15]One novelty in the present analysis compared to [33] is the inclusion of the RG effects also for top quark processes, taking $\mu_f = 2m_t$.

TABLE III. Vector mediators: For the description see the caption of Table II.

Vectors											
Field	Irrep	Normalization	Direction	Top	$b \to s\ell\ell$	ε'/ε	δg_Z	β	Q_W^{Cs}	m_W	Combined
$\mathcal{B} \sim (\mathbf{1},\mathbf{1})_0$	$\mathbf{8}_q$	$-(g_{\mathcal{B}}^q)^2/(12M_{\mathcal{B}}^2)$	$3\mathcal{O}_{qq}^{(1)E} - \mathcal{O}_{qq}^{(1)D}$	1.0	1.5	0.5	0.8	[0.5, 2.7]	0.4	0.5	[1.4, 6.3]
	$\mathbf{8}_u$	$-(g_{\mathcal{B}}^u)^2/(12M_{\mathcal{B}}^2)$	$3\mathcal{O}_{uu}^{E} - \mathcal{O}_{uu}^{D}$	0.8	0.3	0.7	0.5	⋯	0.3	0.5	0.8
	$\mathbf{8}_d$	$-(g_{\mathcal{B}}^d)^2/(12M_{\mathcal{B}}^2)$	$3\mathcal{O}_{dd}^{E} - \mathcal{O}_{dd}^{D}$	0.2	⋯	⋯	⋯	⋯	⋯	⋯	0.2
$\mathcal{B}_1 \sim (\mathbf{1},\mathbf{1})_1$	$(\bar{\mathbf{3}}_d,\mathbf{3}_u)$	$-\lvert g_{\mathcal{B}_1}^{du}\rvert^2/(3M_{\mathcal{B}_1}^2)$	$\mathcal{O}_{ud}^{(1)} + 6\mathcal{O}_{ud}^{(8)}$	1.3	⋯	1.2	[0.3, 3.0]	⋯	0.5	⋯	1.4
$\mathcal{W} \sim (\mathbf{1},\mathbf{3})_0$	$\mathbf{8}_q$	$-(g_{\mathcal{W}}^q)^2/(48M_{\mathcal{W}}^2)$	$3\mathcal{O}_{qq}^{(3)E} - \mathcal{O}_{qq}^{(3)D}$	0.7	1.6	0.4	0.5	1.2	0.5	0.2	1.9
$\mathcal{Q}_1 \sim (\mathbf{3},\mathbf{2})_{\frac{1}{6}}$	$(\bar{\mathbf{3}}_d,\bar{\mathbf{3}}_q)$	$2\lvert g_{\mathcal{Q}_1}^{dq}\rvert^2/(3M_{\mathcal{Q}_1}^2)$	$\mathcal{O}_{qd}^{(1)} - 3\mathcal{O}_{qd}^{(8)}$	1.3	⋯	0.9	0.6	⋯	0.8	0.2	1.3
$\mathcal{Q}_5 \sim (\mathbf{3},\mathbf{2})_{-\frac{5}{6}}$	$(\bar{\mathbf{3}}_u,\bar{\mathbf{3}}_q)$	$2\lvert g_{\mathcal{Q}_5}^{uq}\rvert^2/(3M_{\mathcal{Q}_5}^2)$	$\mathcal{O}_{qu}^{(1)} - 3\mathcal{O}_{qu}^{(8)}$	2.2	0.3	1.2	1.0	0.2	1.2	0.9	2.1
$\mathcal{Y}_1 \sim (\bar{\mathbf{6}},\mathbf{2})_{\frac{1}{6}}$	$(\bar{\mathbf{3}}_d,\bar{\mathbf{3}}_q)$	$\lvert g_{\mathcal{Y}_1}\rvert^2/(3M_{\mathcal{Y}_1}^2)$	$2\mathcal{O}_{qd}^{(1)} + 3\mathcal{O}_{qd}^{(8)}$	1.4	0.1	1.1	0.7	⋯	0.8	0.2	1.4
$\mathcal{Y}_5 \sim (\bar{\mathbf{6}},\mathbf{2})_{-\frac{5}{6}}$	$(\bar{\mathbf{3}}_u,\bar{\mathbf{3}}_q)$	$\lvert g_{\mathcal{Y}_5}\rvert^2/(3M_{\mathcal{Y}_5}^2)$	$2\mathcal{O}_{qu}^{(1)} + 3\mathcal{O}_{qu}^{(8)}$	2.2	1.0	0.9	1.0	0.2	1.3	0.9	2.1
$\mathcal{G} \sim (\mathbf{8},\mathbf{1})_0$	$\mathbf{8}_q$	$-(g_{\mathcal{G}}^q)^2/(144M_{\mathcal{G}}^2)$	$11\mathcal{O}_{qq}^{(1)D} - 9\mathcal{O}_{qq}^{(1)E} + 9\mathcal{O}_{qq}^{(3)D} - 3\mathcal{O}_{qq}^{(3)E}$	0.9	0.6	⋯	0.7	[0.7, 3.5]	0.7	0.2	0.9
	$\mathbf{8}_u$	$(g_{\mathcal{G}}^u)^2/(36M_{\mathcal{G}}^2)$	$3\mathcal{O}_{uu}^{E} - 5\mathcal{O}_{uu}^{D}$	0.7	0.2	0.4	0.7	⋯	0.4	0.3	0.8
	$\mathbf{8}_d$	$(g_{\mathcal{G}}^d)^2/(36M_{\mathcal{G}}^2)$	$3\mathcal{O}_{dd}^{E} - 5\mathcal{O}_{dd}^{D}$	⋯	⋯	⋯	⋯	⋯	⋯	⋯	[0.0, 0.4]
$\mathcal{G}_1 \sim (\mathbf{8},\mathbf{1})_1$	$(\bar{\mathbf{3}}_d,\mathbf{3}_u)$	$\lvert g_{\mathcal{G}_1}\rvert^2/(9M_{\mathcal{G}_1}^2)$	$-4\mathcal{O}_{ud}^{(1)} + 3\mathcal{O}_{ud}^{(8)}$	1.1	⋯	0.2	[0.4, 7.6]	⋯	0.7	0.2	1.0
$\mathcal{H} \sim (\mathbf{8},\mathbf{3})_0$	$\mathbf{8}_q$	$-(g_{\mathcal{H}})^2/(576M_{\mathcal{H}}^2)$	$27\mathcal{O}_{qq}^{(1)D} - 9\mathcal{O}_{qq}^{(1)E} - 7\mathcal{O}_{qq}^{(3)D} - 3\mathcal{O}_{qq}^{(3)E}$	0.4	0.7	0.2	0.4	0.8	0.6	0.2	0.9
	1	$(g_{\mathcal{H}})^2/(96M_{\mathcal{H}}^2)$	$2\mathcal{O}_{qq}^{(3)D} + 3\mathcal{O}_{qq}^{(3)E} - 9\mathcal{O}_{qq}^{(1)E}$	0.5	1.0	0.3	0.6	0.5	⋯	0.4	1.0

limit, whereas a reported interval corresponds to a 2σ preferred range.

The results for all scalar mediators are given in Table II. We observe that $b \to s\ell\ell$ plays an important role in constraining the linear combinations of $\mathcal{O}_{qq}^{(1)D,E}$ and $\mathcal{O}_{qq}^{(3)D,E}$ operators. This is most apparent in the cases of $\omega_1 \sim \bar{\mathbf{6}}_q$ and $\Upsilon \sim \mathbf{6}_q$, where the bounds obtained using $b \to s\ell\ell$ reach $\gtrsim$3 TeV. For the $\zeta \sim \mathbf{3}_q$ and $\Omega_1 \sim \bar{\mathbf{3}}_q$, we obtain bounds which are comparable to the tree-level results, still $\gtrsim$2 TeV. On the other hand, ε'/ε bounds turn out to be less stringent, however, for $\varphi \sim (\bar{\mathbf{3}}_q,\mathbf{3}_u)$, $\omega_4 \sim \mathbf{3}_u$ and $\Omega_4 \sim \mathbf{6}_u$, the bounds are still around 1 TeV. Z-pole observables impose significant bounds on the same leading directions constrained by $b \to s\ell\ell$, extending to multi-TeV

TABLE IV. Fermion mediators: For the description see the caption of Table II.

Fermions											
Field	Irrep	Normalization	Direction	Top	$b \to s\ell\ell$	ε'/ε	δg_Z	β	Q_W^{Cs}	m_W	Combined
$U \sim (\mathbf{3},\mathbf{1})_{\frac{2}{3}}$	$\mathbf{3}_q$	$\lvert\lambda_U\rvert^2/(4M_U^2)$	$\mathcal{O}_{\phi q}^{(1)} - \mathcal{O}_{\phi q}^{(3)} + [2y_u^*\mathcal{O}_{u\phi} + \text{H.c.}]$	⋯	2.2	0.6	5.2	[3.1, 15.5]	3.1	1.6	4.3
$D \sim (\mathbf{3},\mathbf{1})_{-\frac{1}{3}}$	$\mathbf{3}_q$	$-\lvert\lambda_D\rvert^2/(4M_D^2)$	$\mathcal{O}_{\phi q}^{(1)} + \mathcal{O}_{\phi q}^{(3)} - [2y_d^*\mathcal{O}_{d\phi} + \text{H.c.}]$	0.2	2.0	0.6	7.5	[3.1, 15.5]	2.1	4.0	6.3
$Q_1 \sim (\mathbf{3},\mathbf{2})_{\frac{1}{6}}$	$\mathbf{3}_u$	$-\lvert\lambda_{Q_1}^u\rvert^2/(2M_{Q_1}^2)$	$\mathcal{O}_{\phi u} - [y_u^*\mathcal{O}_{u\phi} + \text{H.c.}]$	⋯	1.0	0.5	3.2	0.1	2.0	2.3	2.9
	$\mathbf{3}_d$	$\lvert\lambda_{Q_1}^d\rvert^2/(2M_{Q_1}^2)$	$\mathcal{O}_{\phi d} + [y_d^*\mathcal{O}_{d\phi} + \text{H.c.}]$	0.2	⋯	0.5	3.3	⋯	3.3	1.2	4.5
$Q_5 \sim (\mathbf{3},\mathbf{2})_{-\frac{5}{6}}$	$\mathbf{3}_d$	$-\lvert\lambda_{Q_5}\rvert^2/(2M_{Q_5}^2)$	$\mathcal{O}_{\phi d} - [y_d^*\mathcal{O}_{d\phi} + \text{H.c.}]$	0.2	⋯	0.4	1.6	⋯	2.1	0.6	[2.0, 15.4]
$Q_7 \sim (\mathbf{3},\mathbf{2})_{\frac{7}{6}}$	$\mathbf{3}_u$	$\lvert\lambda_{Q_7}\rvert^2/(2M_{Q_7}^2)$	$\mathcal{O}_{\phi u} + [y_u^*\mathcal{O}_{u\phi} + \text{H.c.}]$	⋯	0.5	0.4	2.1	⋯	3.1	4.5	4.7
$T_1 \sim (\mathbf{3},\mathbf{3})_{-\frac{1}{3}}$	$\mathbf{3}_q$	$\lvert\lambda_{T_1}\rvert^2/(16M_{T_1}^2)$	$\mathcal{O}_{\phi q}^{(3)} - 3\mathcal{O}_{\phi q}^{(1)} + [2y_d^*\mathcal{O}_{d\phi} + 4y_u^*\mathcal{O}_{u\phi} + \text{H.c.}]$	0.2	0.6	0.2	2.0	3.6	1.8	3.0	4.2
$T_2 \sim (\mathbf{3},\mathbf{3})_{\frac{2}{3}}$	$\mathbf{3}_q$	$\lvert\lambda_{T_2}\rvert^2/(16M_{T_2}^2)$	$\mathcal{O}_{\phi q}^{(3)} + 3\mathcal{O}_{\phi q}^{(1)} + [4y_d^*\mathcal{O}_{d\phi} + 2y_u^*\mathcal{O}_{u\phi} + \text{H.c.}]$	0.1	0.5	0.2	2.5	3.6	2.8	1.6	3.2

ranges, and in other cases, the bounds are comparable to those derived from top data. Regarding β decays, stringent constraints are obtained from $\mathcal{O}_{qq}^{(1)D,E}$ and $\mathcal{O}_{qq}^{(3)D,E}$ operators. In the case of $\zeta \sim \mathbf{3}_q$ and $\Upsilon \sim \mathbf{6}_q$, β decays provide a highly competitive lower bound on the effective mass, while in the remaining two cases ($\omega_1 \sim \bar{\mathbf{6}}_q$ and $\Omega_1 \sim \bar{\mathbf{3}}_q$), we obtain a preferred range for the effective mass. The APV observable Q_W^{Cs} yields in many cases constraints exceeding 1 TeV, for example $\omega_4 \sim \mathbf{3}_u$, $\zeta \sim \mathbf{3}_q$, and $\Upsilon \sim \mathbf{6}_q$. The modification of m_W, an effect beyond the leading log, is highly relevant for the $\omega_1 \sim \bar{\mathbf{6}}_q$, $\Omega_4 \sim \mathbf{6}_u$, $\Upsilon \sim \mathbf{6}_q$, and $\Phi \sim (\bar{\mathbf{3}}_q, \mathbf{3}_u)$ irreps, where the obtained bounds are $\gtrsim$1 TeV. In summary, the combined fit notably improves the bound for $\omega_1 \sim \bar{\mathbf{6}}_q$ and $\Upsilon \sim \mathbf{6}_q$ compared to using only top data, while in other cases, it yields a modest enhancement of the bounds, although the RG-induced observables are competitive.

Numerical results for the vector mediators are presented in Table III. Highly important bounds due to $b \to s\ell\ell$ are set for $\mathcal{B} \sim \mathbf{8}_q$, $\mathcal{W} \sim \mathbf{8}_q$, and $\mathcal{H} \sim \mathbf{1}$. ε'/ε gives a bound above 1 TeV for certain irreps, such as $\mathcal{B}_1 \sim (\bar{\mathbf{3}}_d, \mathbf{3}_u)$ and $\mathcal{Y}_1 \sim (\bar{\mathbf{3}}_d, \bar{\mathbf{3}}_q)$, which are comparable to the bounds from top data. The Z-pole observables, β decays, Q_W^{Cs} and m_W seldom reach the 1 TeV level. However, they are often still comparable to the constraints from top data alone. In some instances, Z-pole observables and β decays provide a preferred range rather than a lower limit for the effective mass.

Lastly, for completeness, in Table IV, we collect the constraints on fermion mediators. Tree-level bounds in Ref. [33] were derived using a combined fit of low-energy observables from Refs. [63,77], exceeding 3 TeV in most cases as shown in Table 9 of Ref. [33]. Our analysis focuses on the most relevant observables from these likelihoods, presented individually. While tree-level effects primarily dominate, RG-induced constraints remain significant. As detailed in Sec. III C, for UV fermion mediators, the modification of m_W at leading-log order proves to be a stringent constraint in most cases, with bounds exceeding 3 TeV for $D \sim \mathbf{3}_q$, $Q_7 \sim \mathbf{3}_u$, and $T_1 \sim \mathbf{3}_q$. For $U \sim \mathbf{3}_q$ and $D \sim \mathbf{3}_q$, it is notable that $b \to s\ell\ell$, an RG-induced constraint, sets a lower limit around 2 TeV. Other constraints, largely at the tree level, are similar to those reported in Ref. [33] with minor differences.

B. Direct searches

This subsection examines the direct search sensitivity for two heavy mediators ($\omega_1 \sim \bar{\mathbf{6}}_q$ and $Q_7 \sim \mathbf{3}_u$) primarily constrained at the EFT level by the RG effects discussed in this paper. We review the relevant LHC collider constraints from single and pair production for both cases.

Consider the scalar diquark $\omega_1 \sim \bar{\mathbf{6}}_q$. Table II shows that for this mediator, the primary EFT constraint arises from

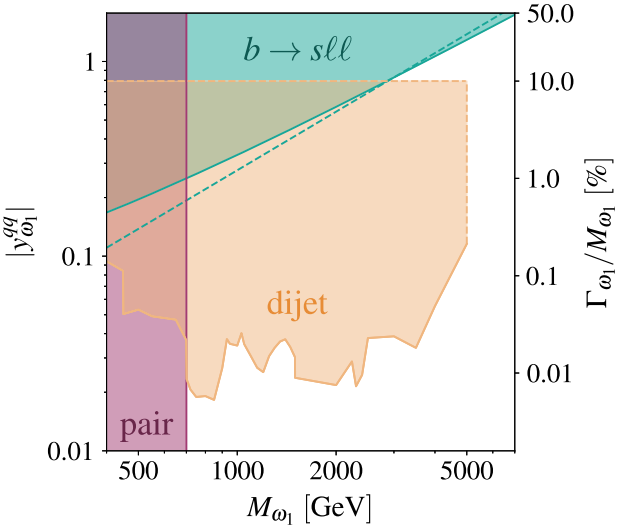

FIG. 2. The leading EFT and direct searches constraints at the 95% CL in the mass-coupling plane of the scalar diquark $\omega_1 \sim \bar{\mathbf{6}}_q$. See Sec. IV B for details.

RG mixing of $\mathcal{O}_{qq}$ into $\mathcal{O}_{\phi q}$, affecting quark FV Z-boson couplings and impacting $b \to s\ell\ell$ processes. The obtained constraint in the coupling versus mass plane ($\mu_i = M_{\omega_1}$) is depicted by the green shaded region in Fig. 2, demonstrating the breaking of the pure power-law dependence on M/y from the previous subsection where $\mu_i = 3$ TeV (dashed green line). For $M_{\omega_1} = 3$ TeV, the two approaches align, but for significantly lower or higher mass values, the discrepancies increase as expected.

The considered diquark couples to gluons and can be pair-produced in proton collisions, with a cross section set by its gauge representation and mass. Considering the ATLAS [78] and CMS [79] searches for pair-produced colored resonances decaying to jets, we obtain a lower limit on the diquark mass of $M_{\omega_1} > 700$ GeV following [80].[16] This constraint is represented in the magenta color in Fig. 2. Moreover, the diquark couples to quark pairs, most notably there is a component of the flavor multiplet that couples to valence quarks.[17] This leads to important constraints from direct searches of dijet resonances from ATLAS [83,84] and CMS [85,86], which have been recast for a generic mediator in Ref. [80]. We use the results from the latter reference to obtain the constraints on Fig. 2 presented in orange. There are two notable abrupt cuts in the shown contour; firstly, the mass interval of the searches stops at

[16]Note that our diquark is a flavor multiplet with 6 mass-degenerate states. We account for an increase of its production cross section by a factor of 6 using the results from Ref. [81].

[17]States coupling to sea and top quarks face suppressed single production due to parton densities. QCD pair production leading to top final states [82] yields bounds comparable to previously discussed jets.

5 TeV at most, explaining the vertical cut in the contour, and secondly, we horizontally cut the contour at the point where the partial decay width of the resonance $\Gamma_{\omega_1} = M_{\omega_1}|y^{qq}_{\omega_1}|^2/(2\pi)$ is equal to 10% of its mass. Above this line, we deem the resonance to be too broad to respect the narrow-width approximation as assumed in obtaining the constraint, and only the EFT constraint applies. Ultimately, we do not consider the parameter space in which the ratio $\Gamma_{\omega_1}/M_{\omega_1} > 50\%$.

The limited parameter space permitted by $b \to s\ell\ell$ and not excluded by direct searches, visible in the upper part of Fig. 2, could be explored through broad (and heavy) resonance searches. This coincides with the region of interest for contact interaction searches in dijet production, which utilize angular distributions [87,88]. Regrettably, the constraints on the WCs obtained in these studies are not directly transferable to our work because the dijet invariant mass underlying these bounds lies in the multi-TeV range, where a mediator-based description is more suitable. A further challenge is that ATLAS and CMS analyze a narrow range of operators, unsuitable even within the restrictive $U(3)^3$ flavor structure. We recommend that experimental collaborations adjust future dijet data interpretations accordingly.

We analyze the vector-like quark $Q_7 \sim \mathbf{3}_u$ for our second example. As Table IV indicates, the most significant EFT constraint is the RG-induced shift in the W-boson mass, imposing a lower limit of over 4.5 TeV on the mass-to-coupling ratio. Concurrently, LHC searches for pair-produced vectorlike quarks, particularly ATLAS, have established a lower bound of 1.3 TeV for top quark partners [89]. This limit applies to the mass of Q_7 since part of its multiplet interacts with the top quark. It is worth noting that single production searches for third-generation vectorlike quarks [90] offer similar, though slightly less stringent probe, due to the parton density suppression. A dedicated search for first-generation vectorlike quarks would be beneficial.

V. CONCLUSION

This paper explores the intricate phenomenology emerging from renormalization group equations in the SMEFT. We rigorously assess the most significant RG mixing patterns by focusing on microscopic theories whose dominant effects are captured with a $U(3)^5$-symmetric dimension-6 operator basis at the UV scale. A key finding is that RG-induced effects on low-energy precision observables often lead to constraints on four-quark (and two-quark) operators that rival or surpass those derived from tree-level processes, notably in top-quark physics. We thoroughly investigate a wide array of single mediator models that match onto the $U(3)^5$-symmetric basis at the tree-level, identified as leading directions. We provide a comprehensive RG analysis of these directions, extending beyond the earlier tree-level study [33]. The key outcomes of this analysis are detailed in three tables; Table II for scalar mediators, Table III for vectors, and Table IV for fermions.

Moving forward, our numerical analysis indicates that the observables we have examined are probing tree-level physics at the TeV scale, characterized by order one couplings, where direct searches can offer complementary probes, as depicted in Fig. 2. A pivotal aspect of future work will be the thorough examination of dijet data within the SMEFT framework and across explicit mediator models, improving the direct search strategies for leading directions, as well as quantifying the validity of the EFT interpretation. Another promising direction is the exploration of $U(2)^5$ flavor symmetry in a similar context. This lower symmetry increases the set of tree-level mediators, adding more complexity and perhaps offering a better benchmark for the physics lying beyond the SM.

ACKNOWLEDGMENTS

This work received funding from the Swiss National Science Foundation (SNF) through the Eccellenza Professorial Fellowship "Flavor Physics at the High Energy Frontier" Project No. 186866.

[1] W. Buchmuller and D. Wyler, Effective Lagrangian analysis of new interactions and flavor conservation, Nucl. Phys. **B268**, 621 (1986).
[2] B. Grzadkowski, M. Iskrzynski, M. Misiak, and J. Rosiek, Dimension-six terms in the standard model Lagrangian, J. High Energy Phys. 10 (2010) 085.
[3] I. Brivio and M. Trott, The standard model as an effective field theory, Phys. Rep. **793**, 1 (2019).
[4] G. Isidori, F. Wilsch, and D. Wyler, The standard model effective field theory at work, arXiv:2303.16922.
[5] G. F. Giudice, C. Grojean, A. Pomarol, and R. Rattazzi, The strongly-interacting light Higgs, J. High Energy Phys. 06 (2007) 045.
[6] B. Henning, X. Lu, and H. Murayama, How to use the standard model effective field theory, J. High Energy Phys. 01 (2016) 023.
[7] B. Henning, X. Lu, T. Melia, and H. Murayama, 2, 84, 30, 993, 560, 15456, 11962, 261485, ...: Higher dimension operators in the SM EFT, J. High Energy Phys. 08 (2017) 016; 09 (2019) 19.

[8] R. Alonso, E. E. Jenkins, A. V. Manohar, and M. Trott, Renormalization group evolution of the standard model dimension six operators III: Gauge coupling dependence and phenomenology, J. High Energy Phys. 04 (2014) 159.
[9] R. K. Ellis *et al.*, Physics briefing book: Input for the European Strategy for Particle Physics Update 2020, arXiv:1910.11775.
[10] A. Greljo, A. Palavrić, and A. E. Thomsen, Adding flavor to the SMEFT, J. High Energy Phys. 10 (2022) 010.
[11] D. A. Faroughy, G. Isidori, F. Wilsch, and K. Yamamoto, Flavour symmetries in the SMEFT, J. High Energy Phys. 08 (2020) 166.
[12] G. D'Ambrosio, G. F. Giudice, G. Isidori, and A. Strumia, Minimal flavor violation: An effective field theory approach, Nucl. Phys. **B645**, 155 (2002).
[13] R. Aoude, T. Hurth, S. Renner, and W. Shepherd, The impact of flavour data on global fits of the MFV SMEFT, J. High Energy Phys. 12 (2020) 113.
[14] S. Bruggisser, D. van Dyk, and S. Westhoff, Resolving the flavor structure in the MFV-SMEFT, J. High Energy Phys. 02 (2022) 225.
[15] R. Bartocci, A. Biekötter, and T. Hurth, A global analysis of the SMEFT under the minimal MFV assumption, arXiv:2311.04963.
[16] C. Grunwald, G. Hiller, K. Kröninger, and L. Nollen, More synergies from beauty, top, Z and Drell-Yan measurements in SMEFT, J. High Energy Phys. 11 (2023) 110.
[17] R. Barbieri, G. Isidori, J. Jones-Perez, P. Lodone, and D. M. Straub, $U(2)$ and minimal flavour violation in supersymmetry, Eur. Phys. J. C **71**, 1725 (2011).
[18] A. L. Kagan, G. Perez, T. Volansky, and J. Zupan, General minimal flavor violation, Phys. Rev. D **80**, 076002 (2009).
[19] J. Fuentes-Martín, G. Isidori, J. Pagès, and K. Yamamoto, With or without U(2)? Probing non-standard flavor and helicity structures in semileptonic B decays, Phys. Lett. B **800**, 135080 (2020).
[20] L. Allwicher, C. Cornella, G. Isidori, and B. A. Stefanek, New physics in the third generation: A comprehensive SMEFT analysis and future prospects, J. High Energy Phys. 03 (2024) 049.
[21] S. Antusch, A. Greljo, B. A. Stefanek, and A. E. Thomsen, U(2) is right for leptons and left for quarks, arXiv:2311.09288.
[22] E. E. Jenkins, A. V. Manohar, and M. Trott, Renormalization group evolution of the standard model dimension six operators II: Yukawa dependence, J. High Energy Phys. 01 (2014) 035.
[23] E. E. Jenkins, A. V. Manohar, and M. Trott, Renormalization group evolution of the standard model dimension six operators I: Formalism and lambda dependence, J. High Energy Phys. 10 (2013) 087.
[24] C. S. Machado, S. Renner, and D. Sutherland, Building blocks of the flavourful SMEFT RG, J. High Energy Phys. 03 (2022) 226.
[25] S. Dawson *et al.*, LHC EFT WG Note: Precision matching of microscopic physics to the standard model effective field theory (SMEFT), arXiv:2212.02905.
[26] J. Aebischer, J. Kumar, and D. M. Straub, Wilson: A PYTHON package for the running and matching of Wilson coefficients above and below the electroweak scale, Eur. Phys. J. C **78**, 1026 (2018).
[27] A. Celis, J. Fuentes-Martin, A. Vicente, and J. Virto, DsixTools: The standard model effective field theory toolkit, Eur. Phys. J. C **77**, 405 (2017).
[28] J. Fuentes-Martin, P. Ruiz-Femenia, A. Vicente, and J. Virto, DsixTools 2.0: The effective field theory toolkit, Eur. Phys. J. C **81**, 167 (2021).
[29] S. Di Noi and L. Silvestrini, RGESolver: A C++ library to perform renormalization group evolution in the standard model effective theory, Eur. Phys. J. C **83**, 200 (2023).
[30] J. Aebischer, J. Kumar, P. Stangl, and D. M. Straub, A global likelihood for precision constraints and flavour anomalies, Eur. Phys. J. C **79**, 509 (2019).
[31] J. J. Ethier, G. Magni, F. Maltoni, L. Mantani, E. R. Nocera, J. Rojo, E. Slade, E. Vryonidou, and C. Zhang (SMEFiT Collaboration), Combined SMEFT interpretation of Higgs, diboson, and top quark data from the LHC, J. High Energy Phys. 11 (2021) 089.
[32] F. Garosi, D. Marzocca, A. Rodriguez-Sanchez, and A. Stanzione, Indirect constraints on top quark operators from a global SMEFT analysis, J. High Energy Phys. 12 (2023) 129.
[33] A. Greljo and A. Palavrić, Leading directions in the SMEFT, J. High Energy Phys. 09 (2023) 009.
[34] J. de Blas, J. C. Criado, M. Perez-Victoria, and J. Santiago, Effective description of general extensions of the standard model: The complete tree-level dictionary, J. High Energy Phys. 03 (2018) 109.
[35] J. Kumar, Renormalization group improved implications of semileptonic operators in SMEFT, J. High Energy Phys. 01 (2022) 107.
[36] E. E. Jenkins, A. V. Manohar, and P. Stoffer, Low-energy effective field theory below the electroweak scale: Operators and matching, J. High Energy Phys. 03 (2018) 016.
[37] T. Hurth, S. Renner, and W. Shepherd, Matching for FCNC effects in the flavour-symmetric SMEFT, J. High Energy Phys. 06 (2019) 029.
[38] A. Greljo, J. Salko, A. Smolkovič, and P. Stangl, Rare b decays meet high-mass Drell-Yan, J. High Energy Phys. 05 (2023) 087,
[39] M. Algueró, A. Biswas, B. Capdevila, S. Descotes-Genon, J. Matias, and M. Novoa-Brunet, To (b)e or not to (b)e: No electrons at LHCb, Eur. Phys. J. C **83**, 648 (2023).
[40] M. Ciuchini, M. Fedele, E. Franco, A. Paul, L. Silvestrini, and M. Valli, Constraints on lepton universality violation from rare B decays, Phys. Rev. D **107**, 055036 (2023).
[41] T. Hurth, F. Mahmoudi, and S. Neshatpour, B anomalies in the post $R_{K^{(*)}}$ era, Phys. Rev. D **108**, 115037 (2023).
[42] D. Guadagnoli, C. Normand, S. Simula, and L. Vittorio, Insights on the current semi-leptonic B-decay discrepancies —and how $B_s \to \mu^+\mu^-\gamma$ can help, J. High Energy Phys. 10 (2023) 102.
[43] R. L. Workman *et al.* (Particle Data Group), Review of particle physics, Prog. Theor. Exp. Phys. **2022**, 083C01 (2022).
[44] R. Abbott *et al.* (RBC, UKQCD Collaborations), Direct CP violation and the $\Delta I = 1/2$ rule in $K \to \pi\pi$ decay from the standard model, Phys. Rev. D **102**, 054509 (2020).

[45] A. J. Buras and J.-M. Gérard, Isospin-breaking in ε'/ε: Impact of η_0 at the dawn of the 2020s, Eur. Phys. J. C **80**, 701 (2020).
[46] J. Aebischer, C. Bobeth, and A. J. Buras, ε'/ε in the standard model at the dawn of the 2020s, Eur. Phys. J. C **80**, 705 (2020).
[47] J. Aebischer, C. Bobeth, A. J. Buras, and J. Kumar, BSM master formula for ε'/ε in the WET basis at NLO in QCD, J. High Energy Phys. 12 (2021) 043.
[48] V. Cirigliano, H. Gisbert, A. Pich, and A. Rodríguez-Sánchez, Isospin-violating contributions to ϵ'/ϵ, J. High Energy Phys. 02 (2020) 032.
[49] J. Aebischer, C. Bobeth, A. J. Buras, J.-M. Gérard, and D. M. Straub, Master formula for ε'/ε beyond the standard model, Phys. Lett. B **792**, 465 (2019).
[50] S. Fajfer, J. F. Kamenik, N. Košnik, A. Smolkovič, and M. Tammaro, New physics in *CP* violating and flavour changing quark dipole transitions, J. High Energy Phys. 10 (2023) 133.
[51] M. Awramik, M. Czakon, A. Freitas, and G. Weiglein, Precise prediction for the W boson mass in the standard model, Phys. Rev. D **69**, 053006 (2004).
[52] L. Berthier and M. Trott, Towards consistent electroweak precision data constraints in the SMEFT, J. High Energy Phys. 05 (2015) 024.
[53] M. Bjørn and M. Trott, Interpreting *W* mass measurements in the SMEFT, Phys. Lett. B **762**, 426 (2016).
[54] E. Bagnaschi, J. Ellis, M. Madigan, K. Mimasu, V. Sanz, and T. You, SMEFT analysis of m_W, J. High Energy Phys. 08 (2022) 308.
[55] D. M. Straub, flavio: A PYTHON package for flavour and precision phenomenology in the standard model and beyond, arXiv:1810.08132.
[56] T. Aaltonen *et al.* (CDF Collaboration), High-precision measurement of the *W* boson mass with the CDF II detector, Science **376**, 170 (2022).
[57] A. Efrati, A. Falkowski, and Y. Soreq, Electroweak constraints on flavorful effective theories, J. High Energy Phys. 07 (2015) 018.
[58] J. de Blas, M. Chala, and J. Santiago, Renormalization group constraints on new top interactions from electroweak precision data, J. High Energy Phys. 09 (2015) 189.
[59] S. Schael *et al.* (ALEPH, DELPHI, L3, OPAL, SLD, LEP Electroweak Working Group, SLD Electroweak Group, SLD Heavy Flavour Group Collaborations), Precision electroweak measurements on the *Z* resonance, Phys. Rep. **427**, 257 (2006).
[60] K. Abe *et al.* (SLD Collaboration), First direct measurement of the parity violating coupling of the Z0 to the s quark, Phys. Rev. Lett. **85**, 5059 (2000).
[61] P. Janot and S. Jadach, Improved Bhabha cross section at LEP and the number of light neutrino species, Phys. Lett. B **803**, 135319 (2020).
[62] A. Freitas, Higher-order electroweak corrections to the partial widths and branching ratios of the Z boson, J. High Energy Phys. 04 (2014) 070.
[63] A. Falkowski, M. González-Alonso, and K. Mimouni, Compilation of low-energy constraints on 4-fermion operators in the SMEFT, J. High Energy Phys. 08 (2017) 123.
[64] M. González-Alonso, O. Naviliat-Cuncic, and N. Severijns, New physics searches in nuclear and neutron β decay, Prog. Part. Nucl. Phys. **104**, 165 (2019).
[65] J. C. Hardy and I. S. Towner, Superallowed $0^+ \to 0^+$ nuclear β decays: 2020 critical survey, with implications for V_{ud} and CKM unitarity, Phys. Rev. C **102**, 045501 (2020).
[66] A. Crivellin, M. Hoferichter, M. Kirk, C. A. Manzari, and L. Schnell, First-generation new physics in simplified models: from low-energy parity violation to the LHC, J. High Energy Phys. 10 (2021) 221.
[67] A. K. Alok, A. Dighe, S. Gangal, and J. Kumar, Leptonic operators for cabbibo angle anomaly with SMEFT RG evolution, Phys. Rev. D **108**, 113005 (2023).
[68] A. Crivellin, F. Kirk, C. A. Manzari, and M. Montull, Global electroweak fit and vector-like leptons in light of the cabibbo angle anomaly, J. High Energy Phys. 12 (2020) 166.
[69] V. Cirigliano, W. Dekens, J. de Vries, E. Mereghetti, and T. Tong, Anomalies in global SMEFT analyses: A case study of first-row CKM unitarity, J. High Energy Phys. 03 (2024) 033.
[70] M. Kirk, Cabibbo anomaly versus electroweak precision tests: An exploration of extensions of the standard model, Phys. Rev. D **103**, 035004 (2021).
[71] C. Patrignani *et al.* (Particle Data Group), Review of particle physics, Chin. Phys. C **40**, 100001 (2016).
[72] P. A. Zyla *et al.* (Particle Data Group), Review of particle physics, Prog. Theor. Exp. Phys. **2020**, 083C01 (2020).
[73] J. Erler and S. Sut, The weak neutral curren, Prog. Part. Nucl. Phys. **71**, 119 (2013).
[74] M. Cadeddu, N. Cargioli, F. Dordei, C. Giunti, and E. Picciau, Muon and electron g-2 and proton and cesium weak charges implications on dark Zd models, Phys. Rev. D **104**, 011701 (2021).
[75] C. S. Wood, S. C. Bennett, D. Cho, B. P. Masterson, J. L. Roberts, C. E. Tanner, and C. E. Wieman, Measurement of parity nonconservation and an anapole moment in cesium, Science **275**, 1759 (1997).
[76] J. Guena, M. Lintz, and M. A. Bouchiat, Measurement of the parity violating 6S-7S transition amplitude in cesium achieved within $2 \times 10(-13)$ atomic-unit accuracy by stimulated-emission detection, Phys. Rev. A **71**, 042108 (2005).
[77] V. Bresó-Pla, A. Falkowski, M. González-Alonso, and K. Monsálvez-Pozo, EFT analysis of new physics at COHERENT J. High Energy Phys. 05 (2023) 074.
[78] M. Aaboud *et al.* (ATLAS Collaboration), A search for pair-produced resonances in four-jet final states at $\sqrt{s} =$ 13 TeV with the ATLAS detector, Eur. Phys. J. C **78**, 250 (2018).
[79] A. M. Sirunyan *et al.* (CMS Collaboration), Search for pair-produced resonances decaying to quark pairs in proton-proton collisions at $\sqrt{s} = 13$ TeV, Phys. Rev. D **98**, 112014 (2018).
[80] M. Bordone, A. Greljo, and D. Marzocca, Exploiting dijet resonance searches for flavor physics, J. High Energy Phys. 08 (2021) 036.

[81] I. Doršner and A. Greljo, Leptoquark toolbox for precision collider studies, J. High Energy Phys. 05 (2018) 126.

[82] A. M. Sirunyan *et al.* (CMS Collaboration), Search for top squarks in final states with two top quarks and several light-flavor jets in proton-proton collisions at $\sqrt{s} = 13$ TeV, Phys. Rev. D **104**, 032006 (2021).

[83] M. Aaboud *et al.* (ATLAS Collaboration), Search for low-mass dijet resonances using trigger-level jets with the ATLAS detector in pp collisions at $\sqrt{s} = 13$ TeV, Phys. Rev. Lett. **121**, 081801 (2018).

[84] G. Aad *et al.* (ATLAS Collaboration), Search for new resonances in mass distributions of jet pairs using 139 fb^{-1} of pp collisions at $\sqrt{s} = 13$ TeV with the ATLAS detector, J. High Energy Phys. 03 (2020) 145.

[85] A. M. Sirunyan *et al.* (CMS Collaboration), Search for narrow and broad dijet resonances in proton-proton collisions at $\sqrt{s} = 13$ TeV and constraints on dark matter mediators and other new particles, J. High Energy Phys. 08 (2018) 130.

[86] A. M. Sirunyan *et al.* (CMS Collaboration), Search for high mass dijet resonances with a new background prediction method in proton-proton collisions at $\sqrt{s} = 13$ TeV, J. High Energy Phys. 05 (2020) 033.

[87] M. Aaboud *et al.* (ATLAS Collaboration), Search for new phenomena in dijet events using 37 fb^{-1} of pp collision data collected at $\sqrt{s} = 13$ TeV with the ATLAS detector, Phys. Rev. D **96**, 052004 (2017).

[88] A. M. Sirunyan *et al.* (CMS Collaboration), Search for new physics in dijet angular distributions using proton–proton collisions at $\sqrt{s} = 13$ TeV and constraints on dark matter and other models, Eur. Phys. J. C **78**, 789 (2018); **82**, 379(E) (2022).

[89] M. Aaboud *et al.* (ATLAS Collaboration), Combination of the searches for pair-produced vector-like partners of the third-generation quarks at $\sqrt{s} = 13$ TeV with the ATLAS detector, Phys. Rev. Lett. **121**, 211801 (2018).

[90] A. Tumasyan *et al.* (CMS Collaboration), Search for single production of a vector-like T quark decaying to a top quark and a Z boson in the final state with jets and missing transverse momentum at $\sqrt{s} = 13$ TeV, J. High Energy Phys. 05 (2022) 093.